Appl Phys B
DOI 10.1007/s00340-008-3153-9

Applied Physics B
Lasers and Optics

ZnO lasing in complex systems with tetrapods

V.M. Markushev · V.V. Ursaki · M.V. Ryzhkov · C.M. Briskina · I.M. Tiginyanu · E.V. Rusu · A.A. Zakhidov

Received: 28 May 2008

Abstract A ZnO structure in the form of a core–shell wire was grown with a modified vapour transport and condensation method. The wire consists of a dense core which may play the role of a waveguide and a shell formed mainly from tetrapod-type crystallites. The high optical quality of the produced ZnO material is confirmed by continuous wave photoluminescence (PL) analysis demonstrating that low-temperature PL is related to the recombination of bound excitons, while room-temperature PL is due to free excitons. Good quality of the crystal structure is demonstrated also by the Raman spectrum. The shell of the wire exhibits room-temperature laser action due to lasing modes in tetrapods under the excitation by nanosecond laser pulses. The nature of the lasing modes is discussed. A simplified model for one of the possible modes is suggested.

PACS 89.20.Bb · 42.60.Jf · 42.70.Hj

V.M. Markushev · M.V. Ryzhkov · C.M. Briskina (✉)
Institute of Radio Engineering and Electronics of RAS,
11, Mokhovaya St., Moscow 125009, Russia
e-mail: chara@mail.cplire.ru
Fax: +7-495-6293678

V.V. Ursaki · I.M. Tiginyanu · E.V. Rusu
Laboratory of Low-Dimensional Semiconductor Structures,
Institute of Applied Physics, Academy of Sciences of Moldova,
Academy str. 5, Chisinau 2028, Moldova

A.A. Zakhidov
NanoTech Institute, University of Texas at Dallas, MS BE26 Box
830688, Richardson, TX 75083-0688, USA

1 Introduction

Oxide semiconductors are typically characterized by outstanding stability and remarkable optoelectronic properties. Among them ZnO is an important semiconducting and piezoelectric material which has high potential for numerous applications such as phosphors, transparent conducting films, field emission devices, varistors, piezoelectric transducers, resonators, and sensors [1, 2]. With a wide band gap of 3.3 eV and large exciton binding energy of 60 meV (excitons being stable at room temperature), ZnO holds also an excellent promise for blue and ultraviolet optical devices [1], including ultraviolet microlasers. Due to the possibility of multiple and switchable growth directions of the wurtzite structure and the high ionicity of its polar surfaces, ZnO provides conditions for the formation of a rich micro/nanostructure diversity (see [3–5] and references therein) many of which may be suitable for lasing. Remarkable lasing properties have been demonstrated with microcrystalline thin films [6–8], arrays of ZnO nanorods [9–17], nanowires [18], nanoneedles [19], and nanobelts [20]. The corresponding emission mechanism is related with the near-band-edge radiative recombination of free excitons (FE, ∼3.26 eV), exciton–exciton scattering (EES, ∼3.18 eV), and electron–hole plasma (EHP, ∼3.14 eV) recombination [20]. The nanolasers based on ZnO structures are promising for diverse applications including optical computing, information storage, and microanalysis [9].

The vapour phase transport and condensation method mediated by vapour–liquid–solid or vapour–solid growth is one of the most cost-effective methods for producing high optical quality ZnO structures [9, 13, 14, 16, 18].

In the present paper a modification of vapour phase transport was applied to produce ZnO nanostructures with a com-

plex morphology specifically suitable for laser action and wave guiding.

2 Experimental

The growth of ZnO complex structures was carried out in a horizontal furnace with an argon/oxygen flow. A mixture of ZnO (99.99%) and graphite (99.999%) powders at molar ratio of 1 : 1 was used as source material placed in an inner quartz tube at the end opposite to the entrance of the gas flow. A temperature profile was set in the furnace with the maximum of 1050°C at the place of the source material and a gradient of 20°C/cm with the temperature decrease in the direction opposite to the gas flow. A Si substrate was placed at the distance of 1 cm up-stream from the source material (i.e. in the direction opposite to the gas flow), as is shown schematically in the inset to Fig. 1a. The growth process was performed during a 1-h period of time.

The morphology and chemical composition microanalysis of samples were studied using a VEGA TESCAN TS 5130MM scanning electron microscope (SEM) equipped with an Oxford Instruments INCA energy dispersive X-ray (EDX) system. Additionally, the quality of samples was investigated with an X-ray diffractometer with a CuK_α radiation and a Renishaw Raman spectrometer.

The continuous wave (cw) photoluminescence (PL) was excited by the 351.1-nm line of an Ar^+ Spectra Physics laser and analyzed with a double spectrometer ensuring the spectral resolution better than 0.5 meV. The samples were mounted on the cold station of a LTS-22-C-330 optical cryogenic system.

The lasing characteristics of the produced ZnO structures were measured at room temperature under the pumping by the third harmonic of a Q-switched Nd:YAG laser (355 nm, ~6 ns, 5 Hz). The pumping energy density was varied from 2 mJ/cm^2 up to 15 mJ/cm^2 with the pumping spot area of 8×10^{-3} cm^2. The image of the pumping spot was focused on the entrance slit of the MDR-23 monochromator with the dispersion of 1.3 nm/mm. The spectra were recorded by a CCD matrix with the size of 8.8×6.6 mm^2 installed in place of the exit slit of the monochromator covering the wavelength interval of 11.8 nm with the dispersion around 0.0085 nm/pixel.

3 Morphology characterization and crystal growth mechanism

A ZnO structure in the form of a large-diameter (around 0.7 mm) wire shown in Fig. 1 was produced with the synthetic set-up used. Since no catalyst is used in the growth

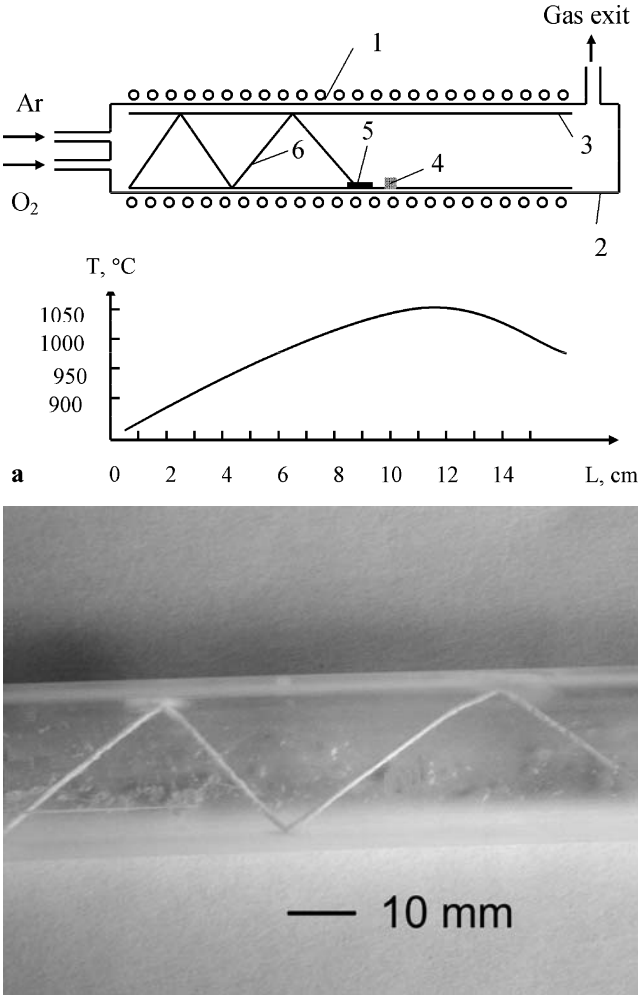

Fig. 1 **a** The schematics of the furnace: *1*—furnace, *2*—quartz reactor, *3*—quartz cylinder, *4*—source material, *5*—Si substrate, *6*—ZnO wire. **b** Photograph of a ZnO wire grown inside quartz tube by vapour transport method

process employed, the mechanism of ZnO structure formation is a vapour–solid process. The Zn vapour is first generated by carbon-induced thermal reduction of ZnO in the high-temperature zone of the furnace. This vapour is then transported upstream of the gas by thermal diffusion due to the temperature gradient of the furnace and Zn is further oxidized by reacting with CO/CO_2 and oxygen from the gas flow. The produced material is deposited in the form of a ZnO wire which starts to grow from the Si substrate surface and propagates in the direction opposite to the gas flow by "reflections" from the walls of quartz tube reactor, as illustrated in Fig. 1.

The produced ZnO microwire consists of a dense core and a crumbly shell formed from ZnO tetrapods. According to the commonly accepted growth model, the gas-phase supersaturation is the dominant factor for the derivation and evolution of the ZnO nanostructure in the vapour–solid

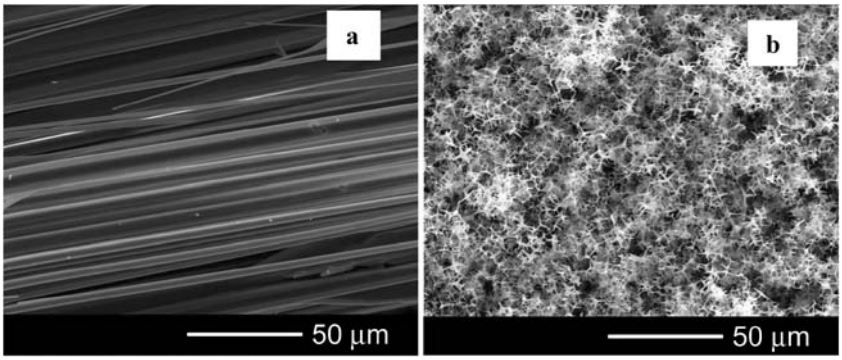

Fig. 2 SEM images of a bold ZnO core (**a**) and a core covered by a dense tetrapod structure (**b**) of ZnO microwire

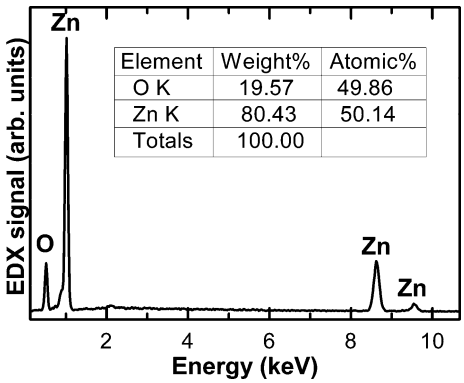

Fig. 3 EDX analysis of the ZnO microwire

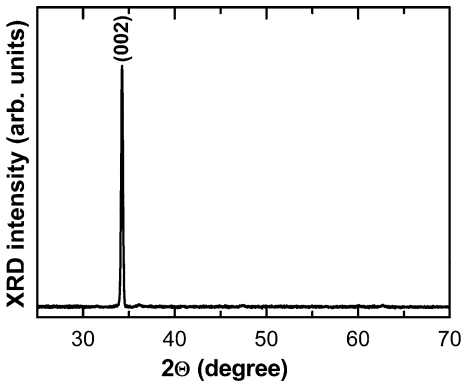

Fig. 4 XRD pattern measured in the cross section of a ZnO microwire core

process [5]. The variations of the gas flow rate lead to fluctuations of the gas-phase supersaturation level, which results in the variation of the density and size distribution of tetrapods in the ZnO wire shell. Therefore, microwires consisting of a more dense bold ZnO core, a core covered by ZnO tetrapods with a moderate density, or high-density tetrapods on the core can be produced with the set-up used as illustrated in Fig. 2.

The EDX analysis of the produced structures demonstrates a stoichiometric ZnO composition in the limits of the sensitivity of the EDX system (Fig. 3).

The X-ray diffraction (XRD) analysis demonstrates a highly directional growth of the core with the (002) axis along the direction of ZnO microwire growth (Fig. 4).

4 Continuous-wave PL and Raman scattering characterization

Note that the cw PL was excited at one end of a segment of the 3-cm-long ZnO microwire and measured at the second end. This demonstrates the good waveguiding properties of the produced microwire. The cw PL spectrum of the ZnO shell is identical to that of the core. The PL of the material produced is dominated by the emission related to the recombination of donor bound excitons (D^0X) [21] and the

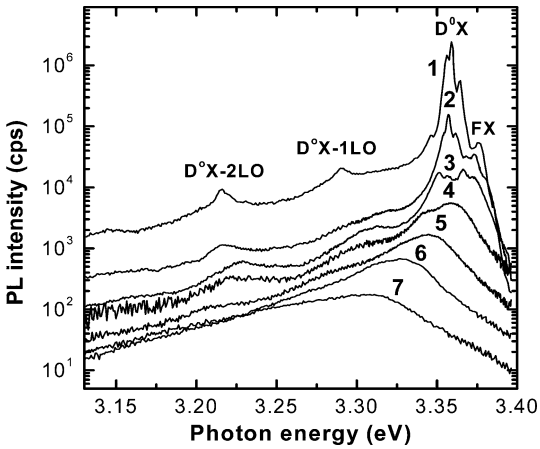

Fig. 5 PL spectra of the ZnO microwire measured at temperatures 10 K (*curve 1*), 50 K (*curve 2*), 100 K (*curve 3*), 150 K (*curve 4*), 200 K (*curve 5*), 250 K (*curve 6*), and 300 K (*curve 7*)

LO phonon replica (Fig. 5). With the increase of the temperature, bound exciton luminescence sharply decreases due to the small value of the excitons' donor-exciton binding energy (as compared to the large value of 60 meV, the internal binding energy of free excitons). As a result, at high temperatures the PL is determined by the recombination of free excitons.

The Raman spectrum of the produced ZnO complex microstructure is illustrated in Fig. 6. This spectrum demonstrates the good quality of the wurtzite crystal structure in the produced material. Wurtzite ZnO belongs to the C_{6v} space group ($P6_3mc$). According to group theory, the corresponding zone centre optical phonons are of the following symmetry modes: $A_1 + 2B_1 + E_1 + 2E_2$ [22]. The $A_1 + E_1 + 2E_2$ modes are Raman active, while $2B_1$ are silent. The low-frequency E_2 mode is predominantly associated with the non-polar vibration of the heavier Zn sublattice, while the high-frequency E_2 mode involves predominantly the displacements of lighter oxygen atoms. The A_1 and E_1 modes are split into LO and TO components. Except for the LO modes, all Raman-active phonon modes are clearly identified in the measured spectrum (Fig. 6).

The LO modes are not visible in the spectrum, likely due to the presence of a high free carrier concentration in the sample. The peak at 331 cm^{-1} is attributed to second-order Raman processes involving acoustic phonons [23]. There are thus several indicatives for a good crystal quality of the produced micro/nanostructures: (i) the signal attributed to the two-phonon density of states (DOS) expected in the spectral range from 500 to 700 cm^{-1} [24, 25] is practically absent; (ii) the peak corresponding to the E_2 (high) mode has a line width of about 5 cm^{-1}, while the line width of the peak corresponding to the E_2 (low) mode is about 2 cm^{-1}, which is comparable to values reported for high-quality ZnO bulk crystals [26]; (iii) the position of the E_2 (high) peak corresponds to the phonon of a bulk ZnO crystal [26], indicating a strain-free state of the micro/nanostructures.

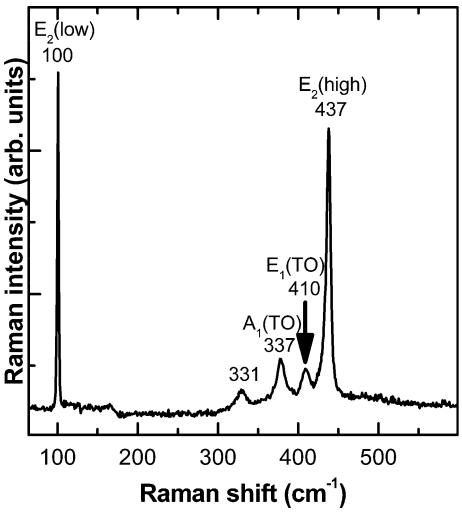

Fig. 6 Raman spectrum of a ZnO microwire measured at room temperature

5 Lasing of the ZnO wire shell

Two samples of complex ZnO structures consisting of wires with shells formed mainly by tetrapods were investigated (Fig. 7). From this figure it follows that the surface density of the tetrapods distribution is approximately 10^7 cm^{-2}. In the first sample (shown in Fig. 7a) the tetrapod sizes are in the interval from ~3 μm up to ~10 μm. The second sample (shown in Fig. 7b) is less uniform, the sizes of the tetrapods being distributed from ~3 μm up to ~25 μm.

A typical emission spectrum measured on a wire with a mere core illustrated in Fig. 2a is presented in Fig. 8. It represents amplified spontaneous emission.

It should be mentioned that, as compared with ZnO nanorods, less attention has been paid to lasing in ZnO tetrapods [27–30]. Particularly, in [27] it was shown that Fabry–Perot-like longitudinal modes account for the lasing spectrum of a single tetrapod leg. However, it seems that all legs contribute to the integral spectrum of a tetrapod. This is confirmed by the modification of the spectrum of an individual tetrapod by removing one of the legs [30].

Our experiments are similar to those recently reported for samples of tetrapods prepared by drop casting of ZnO nanocrystalline powders/ethanol suspension onto various substrates [29]. Nevertheless, there are some significant differences. Particularly, in contrast to results in [29] where no changes of lasing spectra from shot to shot of pumping were registered, we observed a significant variation of lasing spectra. This is illustrated in Fig. 9a and b for sample 1 and sample 2, respectively. Note, that the pumping repetition rate in [29] was 200 Hz, while it is 5 Hz in our experiments.

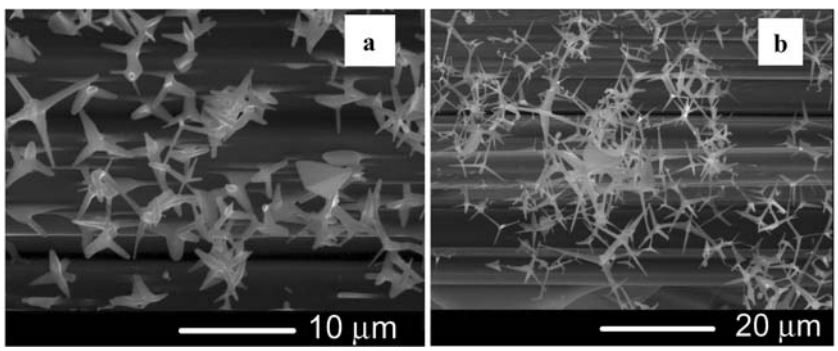

Fig. 7 SEM images of a ZnO sample with a more uniform distribution of tetrapods (**a**) and a less uniform distribution of tetrapods (**b**)

At the same time, the spectra averaged over groups of 30 realizations do not change from one group of realizations to another one (Fig. 10).

One can suggest that the high repetition rate of pumping is responsible for the absence of lasing spectra variations in the previous work [29]. Under such excitation conditions it could be that an individual spectrum registered is a result of pumping by a series of pulses.

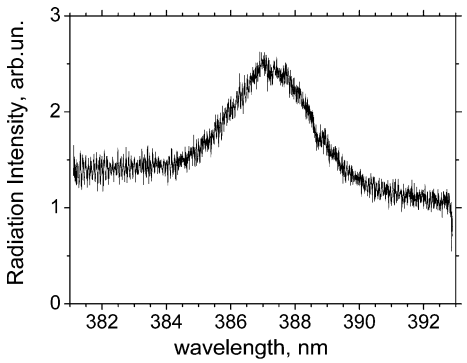

Fig. 8 A typical spectrum of a ZnO wire with a mere core

Analogous variations of lasing spectra from shot to shot were investigated for random lasers on ZnO powders [31]. It was suggested that the random variations of lasing spectra are caused by the fluctuations of spontaneous photon number participating in building up of laser emission of lasing modes. We believe that the nature of lasing spectra variations in the case of tetrapods is the same. Since the sizes of lasing modes in tetrapods are small, the fluctuations of spontaneous photon number may be very significant. However, the analysis of lasing spectra of tetrapods suggests that the lasing mechanism is different from the random lasing by multiple scattering in the shell of the wire formed by tetrapods, it being most probably related to self-supporting cavities of tetrapods.

Figure 11 presents for comparison random lasing spectra of ZnO powder. One can notice that the width of different spectral components in Fig. 7 is noticeably larger as compared to the width of spectral components in Fig. 9. Apart from that, the recurrence of peaks with the same wavelengths in spectra of the tetrapods appears to be much more probable as compared to that of lasing of powder.

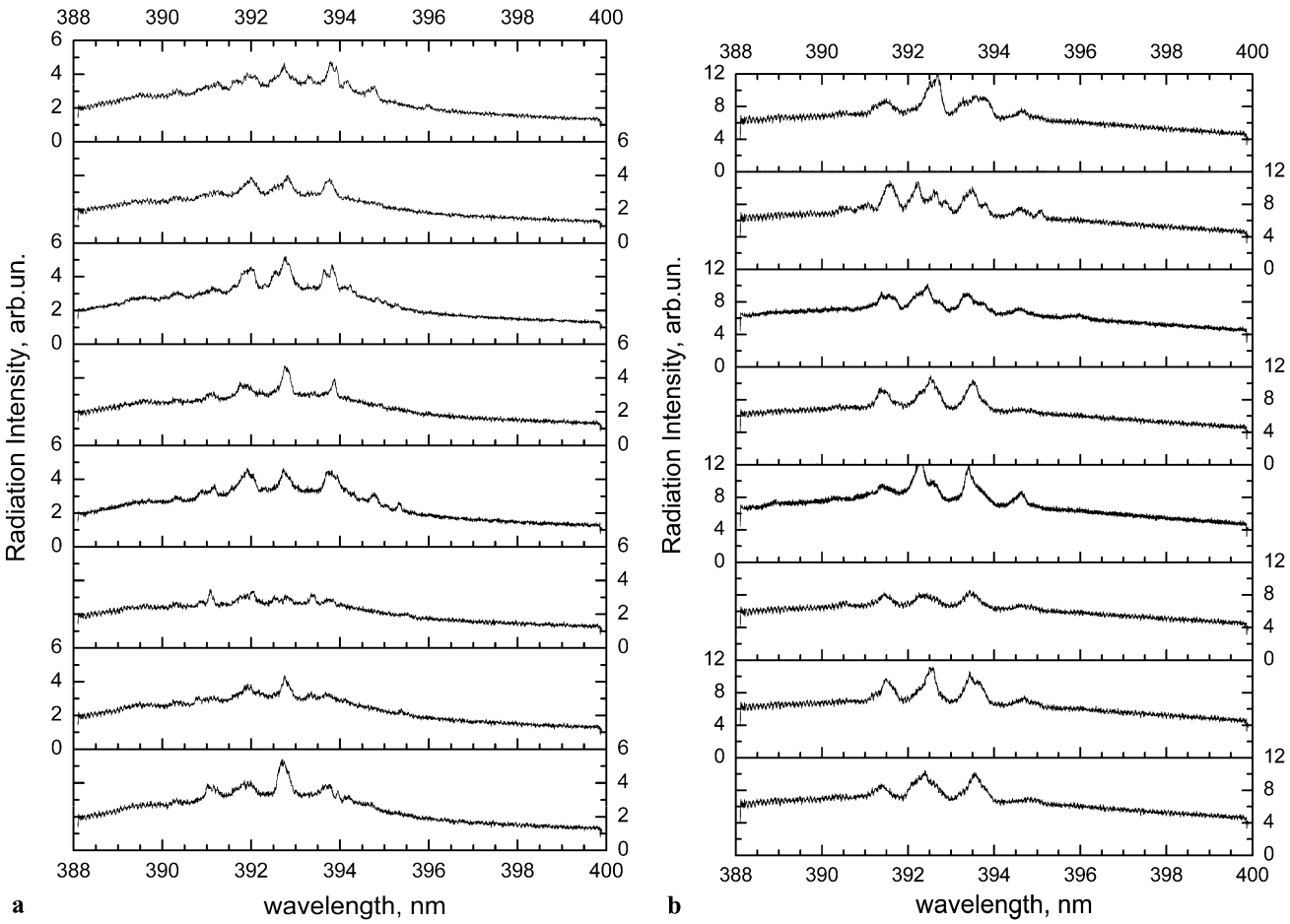

Fig. 9 Examples of lasing spectra variations: **a** sample 1; **b** sample 2

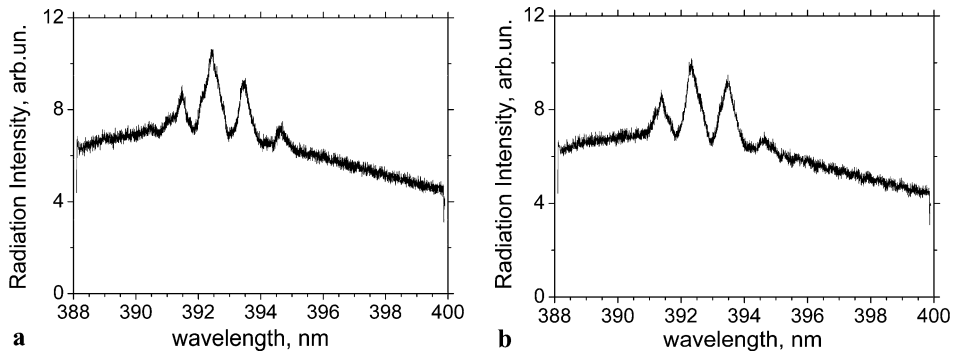

Fig. 10 Lasing spectra averaged over 30 realizations: **a** from 1 up to 30; **b** from 31 up to 60

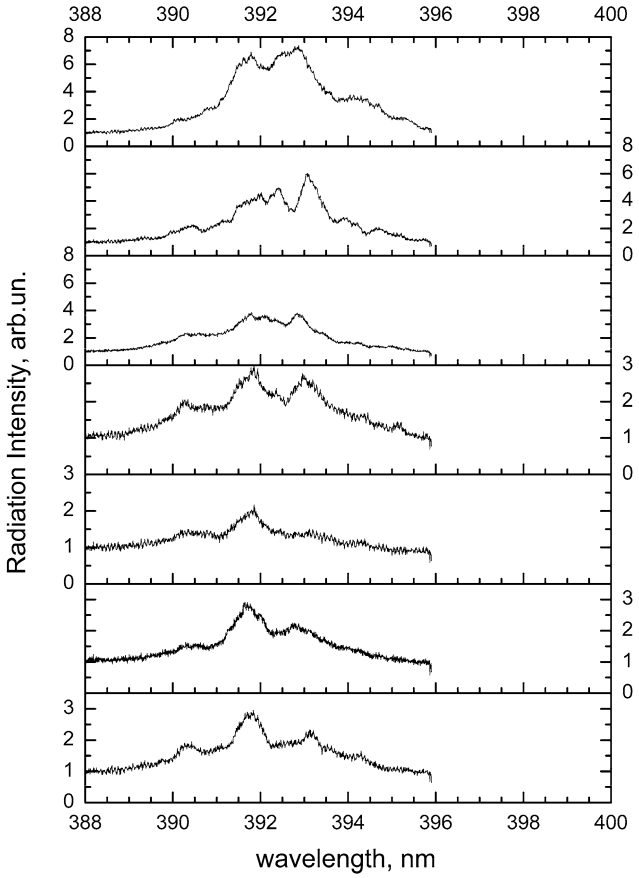

Fig. 11 Examples of random lasing spectra in ZnO powder

The most recurrent lines in the spectrum are those which emerge near the lasing threshold (see the line at 391.58 nm in Fig. 12). This is an expected observation. However, these lines are not the most intensive ones at higher pumping density (Fig. 12b and c). The estimated pumping thresholds are about 2 mJ/cm^2 and 3.4 mJ/cm^2 for samples 1 and 2, respectively. Since the lines usually overlap with each other in the spectrum, it is difficult to estimate the width of single lines. Nevertheless, in some spectra there are lines which do not overlap, as illustrated by the line at 390.76 nm in Fig. 13. The width of this line is quite narrow (∼0.1 nm), demonstrating the existence of high-quality modes in the tetrapods.

The large number of lasing modes (Figs. 12 and 13) results from a large number of tetrapods occurring in the area of the pumping spot. Nevertheless, we believe that the number of modes is still larger than the number of the excited tetrapods, since several modes can be formed in every tetrapod in the spectral range of ZnO excitonic and EHP radiation. We suggest that formation of complex closed photon trajectories in the tetrapod or in its parts can explain the origin of lasing. If the length of these trajectories equals an integral number of wavelengths, they can be considered as a model of modes. Most probably they are formed in the pairs of legs. Since there are six pairs of legs for every tetrapod, at least six modes can exist for every tetrapod.

In Fig. 14 the simple schematics for one of the possible modes is demonstrated. The whole contour is the cross section of a pair of adjacent legs of one tetrapod. The line inside the contour represents a possible photon trajectory which is a result of multiple total internal reflections (TIR). For ZnO in the spectral region considered a minimum angle of TIR is near 25° ($n = 2.45$).

6 Conclusions

The results of this work demonstrate the versatility of the vapour transport and condensation method for the growth of specific ZnO microstructures with unique properties. The modification of the method with a temperature gradient set in the furnace with the temperature decrease in the direction opposite to the Ar and O_2 gas flow results in the growth of a ZnO structure in the form of a microwire that consists of a dense core and an outer overcoat shell formed from randomly grown nanotetrapods. Continuous-wave PL, Raman scattering, EDX, and XRD analysis of the produced complex microstructures demonstrates the high quality of the ZnO material. The core may play the role of a waveguide, while the shell is suitable for laser action. The excitation of the nanostructured shell by nanosecond laser pulses with

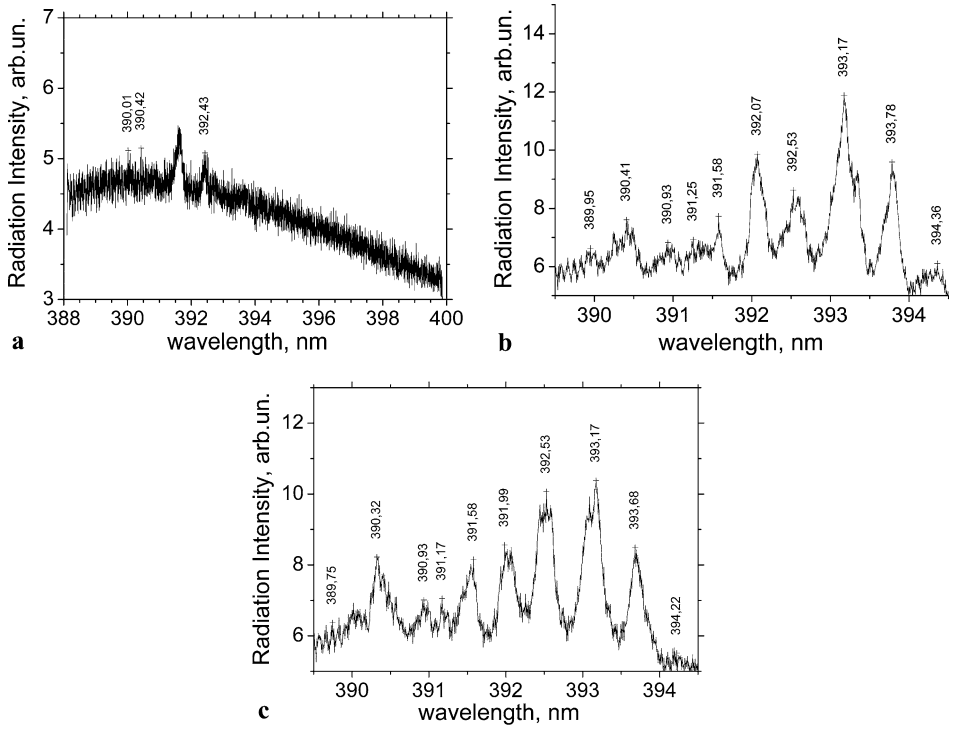

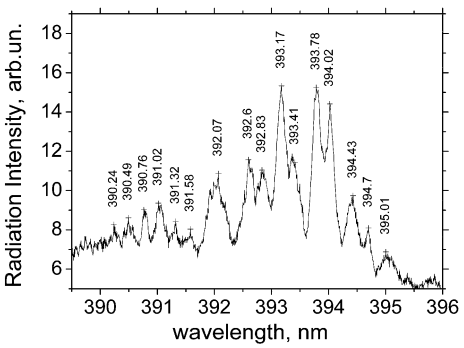

Fig. 13 An example of lasing spectrum with several non-overlapping lines

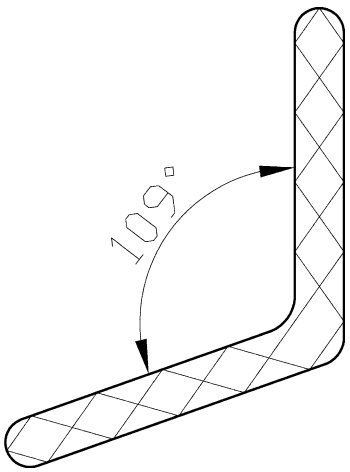

Fig. 14 The scheme of a possible mode

pumping energy density above 2 mJ/cm^2 at room temperature results in lasing with the line width as narrow as 0.1 nm in the region of 388–395 nm. One of the possible explanations of the origin of this narrow lasing mode may be formation of closed photon trajectories by multiple total internal reflections in pairs of tetrapod legs.

Acknowledgements This work is partially supported by STCU under Grant No. 4034, by the Program of basic researches of RAS Presidium, and by the Grant No. RFBR-GFEN 06-02-39016. The authors thank H. Zhong and S.-W. Wang for providing the sample and V.F. Zolin for participating in the paper writing.

References

1. U. Ozgur, Y.I. Aliliv, C. Liu, A. Teke, M.A. Reshchikov, S. Dogan, V. Avrutin, S.-J. Cho, M. Morkoc, J. Appl. Phys. **98**, 041301 (2005)
2. C. Jagadish, S.J. Pearton (eds) *Zinc Oxide Bulk, Thin Films and Nanostructures, Processing, Properties and Applications* (Elsevier Science, Amsterdam, 2006)
3. Z.L. Wang, J. Phys.: Condens. Matter **16**, R829 (2004)
4. M.C. Newton, P.A. Warburton, Mater. Today **10**(5), 50 (2007)
5. V.V. Ursaki, E.V. Rusu, A. Sarua, M. Kuball, G.I. Stratan, A. Burlacu, I.M. Tiginyanu, Nanotechnology **18**, 215705 (2007)
6. D.M. Bagnall, Y.F. Chen, Z. Zhu, T. Yao, S. Koyama, M.Y. Shen, T. Gopto, Appl. Phys. Lett. **70**, 2230 (1997)

7. M. Kawasaki, A. Ohtomo, H. Koinuma, Y. Sakurai, Y. Yoshida, Z.K. Tang, P. Yu, G.K.L. Wong, Y. Segawa, Mater. Sci. Forum **264–268**, 1459 (1998)
8. Z.K. Tang, G.K.L. Wong, P. Yu, M. Kawasaki, A. Ohtomo, H. Koinuma, Y. Segawa, Appl. Phys. Lett. **72**, 3270 (1998)
9. M.H. Huang, S. Mao, H. Feick, H. Yan, Y. Wu, H. Kind, E. Weber, R. Russo, P. Yang, Science **292**, 1897 (2001)
10. Z. Qiu, K.S. Wong, M. Wu, W. Lin, H. Xu, Appl. Phys. Lett. **84**, 2739 (2004)
11. T. Okada, K. Kawashima, M. Ueda, Appl. Phys. A: Mater. Sci. Process. **81**, 907 (2005)
12. Y. Zhang, R.E. Russo, S.S. Mao, Appl. Phys. Lett. **87**, 043106 (2005)
13. X. Han, G. Wang, Q. Wang, L. Cao, R. Liu, B. Zou, J.L. Hou, Appl. Phys. Lett. **86**, 223106 (2005)
14. R. Hauschild, H. Lange, H. Prileer, C. Klingshirn, R. Kling, A. Waag, H.J. Fan, M. Zacharias, H. Kalt, Phys. Status Solidi B **243**, 853 (2006)
15. S.F. Yu, C. Yuen, S.P. Lau, W.I. Park, G.-C. Yi, Appl. Phys. Lett. **84**, 3241 (2004)
16. C.X. Xu, X.W. Sun, C. Yuen, B.J. Chen, S.F. Yu, Z.L. Dong, Appl. Phys. Lett. **86**, 011118 (2005)
17. T. Pauporte, D. Lincot, B. Viana, F. Pelle, Appl. Phys. Lett. **89**, 233112 (2006)
18. H.C. Hsu, C.-Y. Wu, W.-F. Hsieh, Appl. Phys. Lett. **97**, 064315 (2005)
19. S.P. Lau, H.Y. Yang, S.F. Yu, H.D. Li, M. Tanemura, T. Okita, H. Hatano, H.H. Hng, Appl. Phys. Lett. **87**, 013104 (2005)
20. H.D. Li, S.F. Yu, S.P. Lau, E.S.P. Leong, Appl. Phys. Lett. **89**, 021110 (2006)
21. V.V. Ursaki, I.M. Tiginyanu, V.V. Zalamai et al., Phys. Rev. B **70**, 155204 (2004)
22. A. Kaschner, U. Haboeck, M. Strassburg et al., Appl. Phys. Lett. **80**, 1909 (2002)
23. M. Rajalakshmi, A.K. Arora, B.S. Bendre, S. Mahamuni, J. Appl. Phys. **87**, 2445 (2000)
24. F. Reuss, C. Kichner, Th. Gruber, R. Kling, S. Maschek, W. Limmer, A. Waag, P. Ziemann, J. Appl. Phys. **95**, 3385 (2004)
25. J. Serrano, A.H. Romero, F.J. Manjon, R. Lauck, M. Cardona, A. Rubio, Phys. Rev. B **69**, 094306 (2004)
26. F.G. Manjon, A.H. Romero, F. Widulle, R. Lauck, M. Cardona, Phys. Rev. Lett. **90**, 055510 (2003)
27. J.M. Szarko, J.K. Song, C.W. Blackledge, I. Swart, S.R. Leon, S. Li, Y. Zhau, Chem. Phys. Lett. **404**, 171 (2005)
28. Y.H. Leung, W.M. Kwok, A.B. Djurisic, D.L. Phillips, Nanotechnology **16**, 579 (2005)
29. L.E. Li, L.N. Demianets, Opt. Mater. **30**, 1074 (2008)
30. A.B. Djurisic, W.M. Kwok, Y.H. Leung, W.K. Chan, D.L. Phillips, M.S. Lin, S. Gwo, Nanotechnology **17**, 244 (2006)
31. V.M. Markushev, M.V. Ryzhkov, C.M. Briskina, H. Cao, L.A. Zadorozhnaya, E.I. Givargizov, H. Zhong, S.-W. Wang, W. Lu, Laser Phys. **17**, 1109 (2007)